Title

Lipid Homeostasis Is Maintained by Dual Targeting of the Mitochondrial PE Biosynthesis Enzyme to the ER

Journal

Developmental Cell, 44(2)

ISSN

1534-5807

Authors

Friedman, Jonathan R
Kannan, Muthukumar
Toulmay, Alexandre
et al.

Publication Date

2018

DOI

10.1016/j.devcel.2017.11.023

Peer reviewed

HHS Public Access

Author manuscript

Dev Cell. Author manuscript; available in PMC 2019 January 22.

Published in final edited form as:

Dev Cell. 2018 January 22; 44(2): 261–270.e6. doi:10.1016/j.devcel.2017.11.023.

Lipid homeostasis is maintained by dual targeting of the mitochondrial PE biosynthesis enzyme to the ER

Jonathan R. Friedman[1], **Muthukumar Kannan**[2], **Alexandre Toulmay**[2], **Calvin H. Jan**[3,4,5], **Jonathan S. Weissman**[3,4], **William A. Prinz**[2], and **Jodi Nunnari**[1,*]

[1]Department of Molecular and Cellular Biology, University of California, Davis, CA, 95616, USA

[2]Laboratory of Cell and Molecular Biology, National Institute of Diabetes and Digestive and Kidney Diseases, NIH, Bethesda, MD, 20892, USA

[3]Department of Cellular and Molecular Pharmacology, University of California at San Francisco, San Francisco, CA, 94158, USA

[4]Howard Hughes Medical Institute, University of California at San Francisco, San Francisco, CA, 94158, USA

[5]Calico Life Sciences LLC, South San Francisco, CA, 94080, USA

Summary

Spatial organization of phospholipid synthesis in eukaryotes is critical for cellular homeostasis. The synthesis of phosphatidylcholine, the most abundant cellular phospholipid, occurs redundantly via the ER-localized Kennedy pathway and a pathway that traverses the ER and mitochondria via membrane contact sites (MCSs). The basis of the ER-mitochondrial PC synthesis pathway is the exclusive mitochondrial localization of a key pathway enzyme, phosphatidylserine decarboxylase Psd1, which generates phosphatidylethanolamine (PE). We find that Psd1 is localized to both mitochondria and the ER. Our data indicate that Psd1-dependent PE made at mitochondria and the ER has separable cellular functions. In addition, the relative organellar localization of Psd1 is dynamically modulated based on metabolic needs. These data reveal a critical role for ER-localized Psd1 in cellular phospholipid homeostasis, question the significance of an ER-mitochondrial PC synthesis pathway to cellular phospholipid homeostasis, and establish the importance of fine spatial regulation of lipid biosynthesis for cellular functions.

eTOC blurb

Friedman et al. provide evidence that contrary to previous assumption, the phospholipid biosynthesis enzyme Psd1 is localized to both the mitochondria and ER to generate functionally

*correspondance to: jmnunnari@ucdavis.edu.
Lead contact;

Author Contributions:
JF designed and performed experiments and wrote and edited manuscript. MK and AT performed experiments. CJ, WP, and JSW designed experiments and edited manuscript. JN designed experiments and wrote and edited manuscript.

distinct pools of phosphatidylethanolamine. This suggests that, in addition to selective mitochondria-ER lipid transport, localized lipid biosynthesis is significant to organellar identity and function.

Introduction

Phospholipid bilayers are a universal feature of cellularity. Their physical and chemical properties are key determinants of subcellular organelle identity and function in eukaryotic cells. Phosphatidylcholine (PC) and phosphatidylethanolamine (PE) are the primary lipid components of biological membranes and in eukaryotes are synthesized by enzymes localized primarily at the ER via redundant de novo and salvage pathways (Klug and Daum, 2014; van Meer et al., 2008). The prevailing view is that a significant pool of cellular PC can also made de novo from phosphatidylserine (PS) in a pathway that originates in the ER and passes into and out of the mitochondrion (Flis and Daum, 2013) (Fig. 1A). Specifically, ER-derived PS is transported to mitochondria, converted to PE and transported back to the ER where it undergoes trimethylation to generate PC. The PE biosynthesis enzyme in this pathway is the PS decarboxylase Psd1, an inner mitochondrial membrane (IMM)-anchored two-subunit (α/β) complex generated by an autocatalytic proteolytic event required for its function (Horvath et al., 2012). Evidence suggests that PS transport from the ER to mitochondria occurs at membrane contact sites (MCSs) (Achleitner et al., 1995; Ardail et al., 1993; Kornmann et al., 2009; Vance, 1990). PS transport between the outer mitochondrial membrane (OMM) and IMM is catalyzed by Ups2/PRELI-like protein in the intermembrane space (Aaltonen et al., 2016). The molecular basis of retrograde PE transport made from PS by Psd1 from mitochondria to the ER is not known, but also is postulated to occur via MCSs (Ardail et al., 1993; Vance, 1990).

Psd1 functions redundantly to maintain cellular PE pools with the endosome-localized PS decarboxylation enzyme Psd2 and the ER-localized CDP-ethanolamine branch of the Kennedy pathway (Birner et al., 2001; Gulshan et al., 2010; Trotter and Voelker, 1995) (Fig. 1A). In the absence of Psd2 and Dpl1, which degrades phosphorylated sphingoid bases to generate ethanolamine used by the Kennedy pathway, Psd1 is the only source of cellular PE and generates sufficient amounts to support PC biogenesis and maintain cell viability. In contrast, Δ*dpl1*Δ*psd2*Δ*psd1* yeast cells cannot survive except in the presence of exogenous ethanolamine, which can be utilized directly to fuel the Kennedy pathway for PE biosynthesis (Birner et al., 2001).

Psd1 also has an indispensable role in mitochondrial functions (Gohil et al., 2005). Cells lacking Psd1 have abnormal mitochondrial morphology and defects in cellular respiration due to selective depletion of the mitochondrial PE pool (Chan and McQuibban, 2012; Joshi et al., 2012; Kuroda et al., 2011). However, PE generated by the Kennedy pathway can partially suppress respiratory and mitochondrial PE deficiency in *psd1* cells, indicating that PE can also be transported from other organelles into mitochondria (Baker et al., 2016; Chan and McQuibban, 2012). Evidence suggests that MCSs between mitochondria and the ER or mitochondria and vacuoles may also be a source of mitochondrial PE, but the mechanism of PE import is poorly understood (Elbaz-Alon et al., 2014).

A central tenet of the ER-mitochondrial PE-to-PC biosynthesis model is the strictly mitochondrial localization of Psd1. Insight into organelle proteomes can be obtained from proximity-specific ribosome profiling analysis, which enables the quantitative monitoring of localized protein synthesis at organelles (Jan et al., 2014). Proximity analysis of translating ribosomes spatially linked to the ER or mitochondria indicates that the majority of translating proteins is uniquely targeted to their respective organelle (Williams et al., 2014). However, a few proteins were identified whose translation occurs on ribosomes in proximity to both organelles. These include Osm1, a fumarate reductase, which is dually targeted to mitochondria and the ER via signal sequences created by alternative translation start sites (Williams et al., 2014) and Psd1, which is imported and targeted to the IMM via a bipartite signal sequence comprised of a canonical mitochondrial targeting sequence (MTS) and transmembrane domain region (TMR) (Horvath et al., 2012) (Fig. 1B). This observation suggests that, like Osm1, Psd1 exhibits dual mitochondrial and ER localization.

Here, our analysis indicates that the TMR of Psd1 is both necessary and sufficient for dual targeting of Psd1 to mitochondria and ER membranes. Using engineered Psd1 variants that localize exclusively to ER or mitochondria, we find that PE synthesized in each organelle possesses separable functions and the relative steady-state amount of Psd1 at each organelle depends on cellular metabolic state. Our findings challenge the relevance of an ER-mitochondrial pathway for PC biosynthesis and indicate the importance of fine spatial regulation of lipid biosynthesis for cellular functions.

Results

Psd1 is dual localized to mitochondria and the ER

To test whether Psd1 is a constituent of both the ER and mitochondria, we examined its localization using confocal fluorescence microscopy in cells co-expressing functional C-terminally EGFP-tagged Psd1 (Psd1-EGFP) from its chromosomal locus and fluorescent ER (mCherry-HDEL) and mitochondria (mito-TagBFP) markers (Fig. 1C and S1A). A majority of Psd1-EGFP co-localized with mito-TagBFP-labeled mitochondria, consistent with its established IMM localization; however, a significant fraction of Psd1 co-localized with mCherry-HDEL-labeled ER at the nuclear envelope and periphery of cells (Fig. 1C and S1B, arrows). We performed mass spectrometry-based proteomic analysis of functional Psd1-3xFLAG (Fig. S1A) purified using anti-FLAG antibodies from crosslinked yeast whole cell lysates and for comparison analyzed Mic60-3xFLAG, a well-characterized IMM protein with similar topology to Psd1 (Rabl et al., 2009). Proteomic analysis of both Psd1 and Mic60 purifications identified primarily mitochondrial proteins as expected (Hoppins et al., 2011). However, two ER-localized proteins, reticulon (Rtn1) and BiP (Kar2), were enriched in Psd1 purifications (Fig. S1C).

We examined whether native untagged Psd1 was localized to the ER by exploiting the observation that Psd1 possesses predicted N-linked glycosylation motifs to ask if it is glycosylated in the ER lumen. Specifically, we assessed whether a Psd1 species was sensitive to treatment of cell extracts with the glycosidase EndoH by SDS-PAGE/Western analysis with anti-Psd1 antibodies specific to the Psd1 β subunit. As previously described, in wild type extracts, anti-Psd1 antibodies detected a predominant Psd1-specific species with a

mass corresponding to the Psd1 β subunit, a product of N-terminal processing by mitochondrial matrix peptidases and C-terminal autocatalytic cleavage (Horvath et al., 2012; Onguka et al., 2015) (Fig. 1D, lane 1, black arrow). We confirmed this identity by comparative analysis of extracts from cells expressing chromosomally integrated wild type Psd1 or the autocatalytically inactive Psd1(S463A) mutant (Horvath et al., 2012; Onguka et al., 2015) (Fig. 1D, lanes 5 and 9; black versus green arrows). Additionally, a fraction of Psd1 was detected migrating as a species larger than the predominant Psd1 β subunit and was sensitive to EndoH treatment (Fig. 1D, lanes 1, 2 and 5, 6; blue arrows). This EndoH-sensitive Psd1 product migrated more slowly than the unprocessed, EndoH insensitive, α/β Psd1(S463A) chimera (Fig. 2B, lanes 5, 6 and 9, 10; compare solid blue and green arrows). However, analysis of extracts expressing the autocatalytically inactive Psd1(S463A) identified an even slower migrating species that was also sensitive to EndoH (Fig. 1D, lanes 9 and 10; red arrows), indicating that autocatalysis is not required for Psd1 glycosylation. To further test whether the glycosylated species of Psd1 represents extra-mitochondrial Psd1, we performed fractionation of whole cell lysates of wild type cells by differential centrifugation. Western analysis of fractions using ER (Sec61) or mitochondrial (Por1) markers indicated that the ER membranes are enriched in the 1000,000g pellet with no detectable mitochondrial membranes as previously described (Wang et al., 2017) (Fig. S1D). In the 100000g pellet, the glycosylated species of Psd1 was also enriched relative to unglycosylated Psd1 as compared to total lysates, consistent with ER localization of a fraction of Psd1 (Fig. S1D–S1E). Together with the proximity-specific ribosome proximity data (Fig. 1B) and cytological observations (Fig. 1C), these observations suggest that a fraction of native Psd1 is localized to the ER.

To further test this, we mutated asparagine residues in predicted Psd1 N-linked glycosylation motifs and analyzed mutant EndoH-treated cell extracts by SDS-PAGE/Western. Western analysis indicated that the EndoH-sensitive Psd1 species in Psd1(N34Q) cell extracts was absent (Fig. 1D, compare lanes 5 and 7; see solid blue arrow). Instead, we observed a fraction of Psd1(N34Q) co-migrating with the EndoH-dependent product observed in wild type extracts (Fig 1D, compare lanes 6 and 7; see dashed blue arrow), consistent with glycosylation of native Psd1 at N34. Psd1(N34Q) supported known Psd1-dependent functions in cells and Psd1(N34Q)-EGFP localized to both the ER and mitochondria in a similar manner as observed for Psd1-EGFP in cells (Fig. S1F–S1G). Together, these data indicate that a significant fraction of native Psd1 localizes to the ER, where it undergoes autocatalytic processing and glycosylation with its N-terminus exposed to the ER lumen.

The transmembrane domain region of Psd1 is necessary and sufficient for dual targeting

We examined the mechanism of dual Psd1 targeting to mitochondria and the ER. Mutational analysis of the canonical Psd1 start codon revealed that, unlike Osm1 (Jan et al., 2014), alternative start sites were not likely the basis of dual Psd1 targeting. Thus, we considered the possibility that the Psd1 N-terminal IMM bipartite MTS/TMD targeting sequence may also function in ER targeting (Horvath et al., 2012). To test this, we replaced the Psd1 targeting sequence with the targeting sequence of Mic60, an IMM protein with a similar bipartite MTS/TMD targeting sequence and topology in an EGFP-tagged isoform of Psd1 ($Psd1_{Mic60(MTS+TMR)}$; the TMR is a region that includes the TMD and the preceding protein

sequence excluding the MTS, Fig. 2A). Confocal fluorescence microscopy images of wild type cells expressing $Psd1_{Mic60(MTS+TMR)}$-EGFP had no detectable Psd1 localization to the ER in contrast to cells expressing Psd1-EGFP, suggesting that ER localization is a consequence of the N-terminal bipartite Psd1 targeting sequence (Fig. 2A). To test this and determine the contributions of the MTS and TMR to ER targeting, we replaced either the MTS or TMR Psd1 sequences with those of Mic60 to generate the EGFP-tagged Psd1 isoforms $Psd1_{Mic60(MTS)}$ and $Psd1_{Mic60(TMR)}$, respectively. Confocal fluorescence microscopy revealed that only cells expressing $Psd1_{Mic60(MTS)}$, but not $Psd1_{Mic60(TMR)}$, possessed detectable co-localization with an ER marker, suggesting the Psd1 TMR is necessary for its dual localization (Fig. 2A).

To determine if the Psd1 TMR is sufficient for ER-localization, we replaced the Mic60 targeting sequence with the bipartite, MTS and TMD targeting sequences of Psd1 in a EGFP-tagged isoform of Mic60-EGFP to generate $Mic60_{Psd1(MTS+TMR)}$, $Mic60_{Psd1(MTS)}$, and $Mic60_{Psd1(TMR)}$, respectively. Consistent with previous observations, confocal fluorescence microscopy of cells expressing wild type Mic60-EGFP indicated that it localized exclusively within mitochondria (Fig. 2B) (Friedman et al., 2015; Hoppins et al., 2011). Confocal fluorescence microscopy of cells expressing $Mic60_{Psd1(MTS+TMR)}$ revealed that it co-localized with both ER and mitochondrial markers, indicating that the N-terminal bipartite MTS and TMD of Psd1 is sufficient for dual localization (Fig. 2B). Consistent with observations made with $Psd1_{Mic60(MTS)}$ and $Psd1_{Mic60(TMR)}$, ER localization was only observed in cells expressing $Mic60_{Psd1(TMR)}$ and not $Mic60_{Psd1(MTS)}$ (Fig. 2B). Together, these data suggest that the Psd1 TMR is both necessary and sufficient for Psd1 localization to the ER.

Mitochondrial Psd1 is required for normal mitochondrial function and ER-localized Psd1 is required for normal cellular PE homeostasis

To examine the functional significance of dual ER- and mitochondrial-localized Psd1, we utilized $Psd1_{Mic60(MTS+TMR)}$ (hereafter $Psd1_{mito}$) and a Psd1 isoform targeted to the ER ($Psd1_{ER}$) by replacing the Psd1 MTS and TMR with the N-terminal TMD of the ER protein Sec66 (Feldheim et al., 1993; Kurihara and Silver, 1993) (Fig. 3A). We examined the localization of EGFP-tagged $Psd1_{mito}$ and $Psd1_{ER}$ in Δ*psd1* yeast cells by confocal fluorescence microscopy. In contrast to native Psd1, $Psd1_{mito}$ and $Psd1_{ER}$ co-localized exclusively with mitochondria or ER markers, respectively, with no detectable dual targeting (Fig. 3B). By SDS-PAGE/Western analysis, $Psd1_{mito}$ and $Psd1_{ER}$ were expressed at similar levels to wild type Psd1 and were appropriately processed as assessed by comparison to autocatalysis-deficient variants (Fig. S2A), in accordance with previously published work (Horvath et al., 2012; Onguka et al., 2015). Consistent with our cytological data indicating exclusive targeting of $Psd1_{ER}$ and $Psd1_{mito}$, Western analysis identified an EndoH-dependent product in extracts from cells expressing Psd1 and $Psd1_{ER}$ (Fig. S2B). In addition, in vitro analysis of serine decarboxylase activity in extracts from cells in which Psd1 is the sole source of such activity indicates that $Psd1_{ER}$ and $Psd1_{mito}$ possessed comparable, albeit less, activity relative to Psd1 in cells (Fig. S2C). Consistently, cells expressing $Psd1_{ER}$ or $Psd1_{mito}$ supported PS to PE conversion, though at a reduced rate as compared to cells expressing wild type Psd1 (Fig. S2D). These data indicate that $Psd1_{ER}$ and $Psd1_{mito}$ are

specifically targeted to their respective organelles and correctly processed to yield active enzymes.

We asked whether $Psd1_{ER}$ and/or $Psd1_{mito}$ was sufficient to perform the primary cellular functions of Psd1: production of cellular PE and normal mitochondrial morphology and cellular respiration (Baker et al., 2016; Chan and McQuibban, 2012; Joshi et al., 2012; Kuroda et al., 2011). Expression of $Psd1_{mito}$ in Δ*psd1* cells restored both normal mitochondrial morphology, as assessed by confocal fluorescence microscopy of cells expressing mito-GFP, and respiratory function, measured by cell growth on media containing the non-fermentable carbon sources ethanol and glycerol, as compared to wild type cells (Fig. 3C–3E and Fig. S2E). In contrast, expression of $Psd1_{ER}$ in Δ*psd1* cells only partially restored wildtype mitochondrial morphology and respiratory function, consistent with published data (Fig. 3C–3E). Thus, PE synthesized within mitochondria, but not the ER, is both necessary and sufficient to support normal Psd1-dependent mitochondrial functions.

We examined the roles of $Psd1_{ER}$ and/or $Psd1_{mito}$ in extra-mitochondrial cellular PE homeostasis. In the absence of Psd2 and Dpl1, Psd1 is the only source of cellular PE and is thus essential for cell viability unless growth media is supplemented with exogenous ethanolamine to fuel PE production via the Kennedy pathway (Fig. 3F). We compared the growth rate of Δ*dpl1*Δ*psd2*Δ*psd1* yeast cells expressing $Psd1_{ER}$ or $Psd1_{mito}$ on the fermentable carbon source, glucose. As in Δ*psd1* cells, EGFP-tagged $Psd1_{mito}$ and $Psd1_{ER}$ co-localized exclusively with mitochondria or ER markers, respectively, in Δ*dpl1*Δ*psd2*Δ*psd1* yeast cells as assessed by confocal fluorescence microscopy (Fig. S2G). $Psd1_{ER}$ supported growth of Δ*dpl1*Δ*psd2*Δ*psd1* cells, similar to wild type Psd1 and in a manner dependent on Psd1 activity, as previously reported and consistent with our data indicating that native ER-localized Psd1 is auto-catalytically processed and active (Onguka et al., 2015) (Fig. 3F and Figs. S2A–S2D, S2F, S3A). However, similar to our observations in Δ*psd1* cells (Fig. 3C–3D), $Psd1_{ER}$ expressed in Δ*dpl1*Δ*psd2*Δ*psd1* cells failed to support normal mitochondrial morphology in the presence of exogenous ethanolamine (Figs. S3G and S4A-S4B). By contrast, expression of $Psd1_{mito}$ failed to fully rescue the ethanolamine auxotrophy of Δ*dpl1*Δ*psd2*Δ*psd1* cells, which exhibited an approximate 2-fold defect in growth rate, but supported normal respiration and mitochondrial morphology in the presence of ethanolamine (Fig. 3F and Fig. S4A–S4B). The inability of $Psd1_{mito}$ to support wildtype growth of cells reliant on Psd1 for PE production was a consequence of an absent Psd1 TMR, as the growth defect of Δ*dpl1*Δ*psd2*Δ*psd1* cells expressing $Psd1_{mito}$ phenocopied cells expressing $Psd1_{Mic60(TMR)}$ (Fig. S3C–S3D). Steady state analysis of total cellular lipids from Δ*dpl1*Δ*psd2*Δ*psd1* cells expressing Psd1 variants grown without exogenous ethanolamine indicated that $Psd1_{ER}$ supported normal total cellular phospholipid homeostasis (Fig. 3G). In contrast, in cells expressing $Psd1_{mito}$, PE comprised only ~10% of the total cellular lipid composition, significantly less than cells expressing wild type Psd1. Together with the observed ethanolamine auxotrophy of $Psd1_{mito}$-expressing cells, these data suggest that cells lacking the native pool of ER-localized Psd1 are selectively deficient in PE and consequently have a homeostatic imbalance in cellular phospholipid composition.

We reasoned that reduced steady state PE at the ER could explain the growth defect of Δ*dpl1*Δ*psd2*Δ*psd1* cells dependent on $Psd1_{mito}$ for PE production. To test this, we determined the phospholipid composition of purified mitochondrial and ER membranes from Δ*dpl1*Δ*psd2*Δ*psd1* cells expressing Psd1 variants. Steady state lipid analysis of mitochondrial phospholipids indicated that despite abnormal mitochondrial morphology and reduced respiratory function, cells expressing $Psd1_{ER}$ have similar relative amounts of mitochondrial PE as compared to mitochondria from cells expressing either wild type Psd1 or $Psd1_{mito}$ (Fig. 4A). These data suggest that PE produced in the ER can traffic to mitochondria, but to support normal mitochondrial morphology and respiration, PE must be produced within mitochondria, suggesting that locally synthesized mitochondrial PE by Psd1 is unique in terms of either its distribution and/or composition. Consistent with this idea, addition of $Psd1_{mito}$ to Δ*dpl1*Δ*psd2*Δ*psd1* cells expressing $Psd1_{ER}$ restored normal mitochondrial morphology and respiratory function (Fig. S3E–S3G).

In contrast to mitochondrial membranes, cells reliant on $Psd1_{mito}$ for PE synthesis had significantly lower relative amounts of PE in the ER compared to Δ*dpl1*Δ*psd2*Δ*psd1* cells expressing Psd1 or $Psd1_{ER}$ (Fig. 4B). Δ*psd1*Δ*psd2* cells grown with media supplemented only with choline to fuel PC synthesis via the Kennedy pathway are also severely deficient for PE at the ER, consistent with previously published data (Trotter and Voelker, 1995) (Fig. 4B). We thus compared the growth rates of Δ*dpl1*Δ*psd2*Δ*psd1* cells expressing $Psd1_{mito}$ and Δ*psd1*Δ*psd2* cells supplemented with choline. Significantly, compared to wild type cells, the growth defect of Δ*dpl1*Δ*psd2*Δ*psd1* cells expressing $Psd1_{mito}$ phenocopied that of Δ*psd1*Δ*psd2* cells supplemented with choline (Fig. S3B). In the absence of ethanolamine, the relatively slower growth rate of cells dependent on $Psd1_{mito}$ for PE production was exacerbated selectively by deletion of *IRE1*, which encodes the key ER sensor and mediator of the ER unfolded protein response (UPR) pathway (Gardner et al., 2013) (Fig. 4C). *IRE1* deletion also reduced the growth rate of cells dependent on $Psd1_{ER}$ for PE production, however, in contrast to cells expressing $Psd1_{mito}$, the growth defect was similar in the absence or presence of ethanolamine (Fig. 4C). These observations suggest that the observed growth defect of cells lacking ER-localized Psd1 is a consequence of ER dysfunction. In this context, we also observed that in Δ*dpl1*Δ*psd2*Δ*psd1* cells expressing $Psd1_{mito}$, abnormal mitochondrial morphology was observed in the absence of ethanolamine (Fig. S4A–S4B). We speculate this phenotype is a secondary consequence of cell stress dependent on ER dysfunction as addition of $Psd1_{ER}$ to Δ*dpl1*Δ*psd2*Δ*psd1* cells expressing $Psd1_{mito}$ supported normal mitochondrial morphology and respiratory function in the absence of ethanolamine (Figs. S3E–S3G). Consistently, Δ*dpl1*Δ*psd2*Δ*psd1* cells expressing both $Psd1_{ER}$ and $Psd1_{mito}$ were not auxotrophic for ethanolamine (Fig. S3E–S3G), further indicating that Psd1-mediated PE production in the ER is necessary to support normal cell growth when PE cannot be made by the Kennedy pathway. These data indicate that by virtue of its dual localization, native Psd1 synthesizes distinct PE pools, which play functionally non-redundant roles at mitochondria and the ER.

Steady-state level of ER-localized Psd1 is regulated by growth conditions

Given the separate functions of mitochondrial and ER Psd1, we tested whether steady-state Psd1 localization is physiologically modulated in response to total cellular and

mitochondrial PE demand. Specifically, we determined the relative amount of Psd1 localized to the ER in cells grown in fermentable (dextrose, YPD) versus non-fermentable (ethanol and glycerol, YPEG) carbon sources by comparing the amount of glycosylated Psd1 (ER) to total Psd1 (ER and mitochondria) by quantitative Western analysis. Glycosylated Psd1 was significantly enriched in cells grown in YPD compared to cells grown in YPEG media, which requires mitochondrial respiration (Fig. 4D–4E). The anti-correlation of Psd1 localization to the ER with mitochondrial respiratory activity and our data indicating dual targeting of Psd1 is encoded in its TMR suggest mitochondrial import efficiency, which requires mitochondrial membrane potential, may regulate the relative amounts of ER and mitochondrial Psd1. However, in cells treated with the respiratory complex inhibitor antimycin A, which inhibits generation of mitochondrial membrane potential, there was no significant difference in the relative amount of glycosylated Psd1 (Fig. S4C). These data suggest an alternative mechanism by which cells can regulate the dual localization of Psd1. Indeed, we observed a significant increase in the percentage of glycosylated Psd1 in cells grown in less nutritionally rich synthetic media with dextrose (SD) relative to YPD that is dampened by supplementation of wild type or Δ*dpl1*Δ*psd2* yeast cells with exogenous ethanolamine (Fig. 4D–4F). Together, these data indicate that depending on metabolic demand, the steady-state organellar distribution of Psd1 can dynamically change, consistent with distinct physiological roles for mitochondrial- and ER-localized Psd1 (Fig. 4G).

Discussion

Our data indicate that Psd1 localizes to both the ER and mitochondria where it separately contributes to the synthesis of functionally distinct pools of PE. In mitochondria, Psd1 is essential for supporting normal mitochondrial morphology and respiratory function. At the ER, when it is the sole generator of PE, Psd1 is required to synthesize an adequate cellular PE pool and is necessary to maintain optimal PE levels in the ER required for normal ER function. The relative amount of total Psd1 localized to each organelle is modulated by growth conditions that alter the cellular dependence on these separable organelle-specific Psd1-dependent functions.

How metabolic demand controls the relative amounts of Psd1 at the ER and mitochondria is not understood. The region encompassing the TMD of Psd1, embedded within the canonical bipartite mitochondrial signal sequence, is both necessary and sufficient for dual targeting. Thus, one possibility is that this targeting sequence regulates the relative import efficiency into each organelle, although mitochondrial membrane potential, which influences import rate, does not play an apparent role. Alternatively, Psd1 may be constitutively targeted to each organelle and its steady state stability may be regulated. Future studies will be necessary to address both the mechanism and regulation of dual Psd1 targeting.

A well-established mechanism for regulating organelle composition is the selective transport of lipids between cellular membranes. In the absence of redundant pathways for PE synthesis, our data suggest that the rate of retrograde transport of PE generated by mitochondrial Psd1 to the ER is insufficient to meet cellular demands. Thus, our work challenges the dogma of a robust bidirectional PS-PE-PC inter-organellar lipid synthesis pathway. In addition, in light of these data, studies that rely on a strictly mitochondrial

localization of Psd1 to make conclusions regarding lipid transport between mitochondria and the ER and other organelles need to be reevaluated (e.g. (Elbaz-Alon et al., 2014; Kojima et al., 2016; Kornmann et al., 2009; Lahiri et al., 2014; Nguyen et al., 2012)). While our work suggests that PE transport from the mitochondria to the ER is not robust enough to provide cells with a sufficient PE pool, our data indicate PE is robustly transported to mitochondria from extra-mitochondrial sources, but it is insufficient to support mitochondrial function. We speculate that this deficiency may be a consequence of differences in the chemical composition of lipid species selected for transport from the ER to mitochondria, such as fatty acid saturation state (Kainu et al., 2013). This may also be a consequence of differences in intra-mitochondria lipid distribution of ER-transported lipids. Regardless, the demonstration of non-redundant functions of PE generated by Psd1 in mitochondria and the ER illustrate that regulated localized lipid synthesis is an alternative non-transport based mechanism that plays a central role in organellar lipid composition and function.

STAR Methods

CONTACT FOR REAGENT AND RESOURCE SHARING

Further information and requests for resources and reagents should be directed to and will be fulfilled by the Lead Contact, Jodi Nunnari (jmnunnari@ucdavis.edu)

EXPERIMENTAL MODEL AND SUBJECT DETAILS

All yeast strains were constructed in the W303 strain background of *S. cerevisiae* (*ade2-1; leu2-3; his3-11, 15; trp1-1; ura3-1; can1-100*) and were cultured at 23°C or 30°C. For all experiments, strains were cultured where indicated in “Methods Details” below in YPD (1% yeast extract, 2% peptone, 2% glucose), YPEG (1% yeast extract, 2% peptone, 3% glycerol, 3% ethanol), SD (2% glucose, 0.7% yeast nitrogen base, amino acids), or synthetic ethanol/glycerol (3% glycerol, 3% ethanol, 0.7% yeast nitrogen base, amino acids). Where indicated, media was supplemented with 10mM ethanolamine (pH 5.6).

METHOD DETAILS

Plasmids and strain construction—The Δ*psd1* strain was generated by PCR-based homologous recombination replacing the respective ORFs with the NatMX6 cassette. The Δ*dpl1*Δ*psd2* and Δ*dpl1*Δ*psd2*Δ*psd1* strains (Aaltonen et al., 2016) were a gift from T. Langer (CECAD, Cologne). The Δ*psd1*Δ*psd2* strain was generated by replacement of Δ*dpl1* with *DPL1* in Δ*dpl1*Δ*psd2*Δ*psd1* cells. C-terminal -3xFLAG and -EGFP tags of proteins at their endogenous loci were generated using PCR-based homologous recombination with yEGFP::KanMX and 3xFLAG::HIS3MX6 (Hoppins et al., 2011; Sheff and Thorn, 2004) and strains were constructed either directly by lithium acetate transformation or by mating, meiosis and tetrad dissection.

To reintroduce untagged or EGFP-tagged Mic60 or Psd1 variants into wild type, Δ*psd1*, or Δ*dpl1*Δ*psd2*Δ*psd1* strains, each isoform below was cloned into the multiple cloning site of pRS306 (Sikorski and Hieter, 1989) by isothermal assembly and plasmids were linearized by digestion with StuI or EcoRV and integrated into the *ura3-1* locus using lithium acetate transformation.

a. pRS306-Psd1 contains the wild type Psd1 ORF flanked by the native Psd1 promoter and terminator (genomic regions ~500bp upstream and downstream of the *PSD1* locus).

b. pRS306-Psd1-EGFP contains the Psd1 promoter, the wild type Psd1 ORF, a short linker, EGFP, and the terminator from the *ADH* locus.

c. pRS306-Mic60-EGFP was previously described (Friedman et al., 2015).

The following variants were constructed as above with the Psd1 promoter but contain the fusions described instead of the wild type Psd1 ORF:

d. pRS306-Mic60(1-57)-Psd1(102-500), referred to as $Psd1_{mito}$, is a fusion of Mic60 (amino acids 1-57) and Psd1 (amino acids 102-500).

e. pRS306-Mic60(1-57)-Psd1(102-500)-EGFP is referred to as $Psd1_{Mic60(MTS+TMR)}$-EGFP or $Psd1_{mito}$-EGFP.

f. pRS306-Mic60(1-24)-Psd1(57-500)-EGFP is referred to as $Psd1_{Mic60(MTS)}$-EGFP.

g. pRS306-Psd1(1-57)-Mic60(25-57)-Psd1(102-500)-EGFP is referred to as $Psd1_{Mic60(TMR)}$-EGFP.

h. pRS306-Psd1(1-57)-Mic60(25-57)-Psd1(102-500) is referred to as $Psd1_{Mic60(TMR)}$.

i. pRS306-Sec66(1-60)-Psd1(102-500)-EGFP is referred to as $Psd1_{ER}$-EGFP.

j. pRS306-Sec66(1-60)-Psd1(102-500) is referred to as $Psd1_{ER}$.

k. pRS306-Psd1(1-101)-Mic60(58-540)-EGFP is referred to as $Mic60_{Psd1(MTS+TMR)}$-EGFP.

l. pRS306-Psd1(1-57)-Mic60(25-540)-EGFP is referred to as $Mic60_{Psd1(MTS)}$-EGFP.

m. pRS306-Mic60(1-24)-Psd1(57-101)-Mic60(58-540)-EGFP is referred to as $Mic60_{Psd1(TMR)}$-EGFP.

Where noted, the above plasmids were mutagenized to encode Psd1(N34Q) or Psd1(S463A) by site directed mutagenesis.

To express both $Psd1_{mito}$ and $Psd1_{ER}$, Δ*dpl1*Δ*psd2*Δ*psd1* cells expressing $Psd1_{ER}$ integrated at the *ura3-1* locus were transformed with pRS314-Mic60(1-57)-Psd1(102-500) (referred to as $pPsd1_{mito}$), which was generated by subcloning the chimeric Psd1 and flanking regions from pRS306-Mic60(1-57)-Psd1(102-500) into pRS314 (Sikorski and Hieter, 1989).

To visualize mitochondria in cells, the following plasmids were used: pYX142mtGFP (Westermann and Neupert, 2000) and pVT100u-mito-TagBFP (Friedman et al., 2015), described previously, and are referred to as “mito-GFP” and “mito-TagBFP”, respectively. pRS424-mito-TagBFP (also referred to as “mito-TagBFP”) was generated by PCR amplifying mito-mTagBFP flanked by the ADH promoter and terminator from pVT100u mito-mTagBFP and cloning it into the MCS of pRS424 (Sikorski and Hieter, 1989) by

isothermal assembly; this construct was kindly provided by K. Subramanian. To visualize the ER in cells, pRS305-mCherry-HDEL was generated by PCR amplification of the TPI promoter, the Kar2 signal sequence (amino acids 1-45), mCherry with a C-terminal HDEL sequence, and the ADH terminator, followed by isothermal assembly into the multiple cloning site of pRS305 (Sikorski and Hieter, 1989); this plasmid was linearized by EcoRV for integration into the *leu2-3* locus. To immunopurify ER, cells expressing Sec63-HA by introduction of pRS315:Sec63-HA were used (Wang et al., 2017).

Yeast cell growth assays—For comparison of cell growth on dextrose versus ethanol/glycerol plates, cells were grown to exponential phase in YPD, pelleted, and resuspended in water at a concentration of 0.5 OD_{600}/mL. 4μL of 10-fold serial dilutions of cells were plated on YPD and YPEG plates and incubated for ~36h (YPD) and ~48h (YPEG) at 30°C. For comparison of cell growth in the presence of absence of ethanolamine, cells were grown to exponential phase in synthetic dextrose media (SD) supplemented with 10mM ethanolamine, pelleted, and resuspended in water at a concentration of 0.5 OD_{600}/mL. 5μL of 10-fold serial dilutions of cells were plated on SD plates with and without 10mM ethanolamine supplementation and incubated for ~36–48h at 30°C, or 37°C where indicated. To assay growth of Δ*dpl1*Δ*psd2*Δ*psd1* cells expressing both $pPsd1_{mito}$ and $Psd1_{ER}$ on synthetic ethanol/glycerol plates with and without ethanolamine supplementation, plates were incubated for ~96h at 30°C.

To determine doubling time of cells in liquid media, the indicated cells were grown to exponential phase in SD supplemented with 10mM ethanolamine, washed with water, and subsequently grown in SD without ethanolamine; the doubling time was calculated by determining the growth rate of cells between ~OD_{600} 0.3 and 0.9. Growth curve plots were generated using a Bioscreen C (Growth Curves USA). Cells were cultured at 30°C and OD_{600} was measured every 15 minutes.

Whole cell extracts, glycosidase treatment, cellular fractionation, and Western analysis—For whole cell extracts, cells were grown to exponential phase in SD supplemented with 10mM ethanolamine when necessary, or grown in YPD or YPEG when indicated. 0.25 OD_{600} cells were pelleted, washed with dH_20, and extracts were prepared by alkaline extraction (0.255M NaOH, 1% 2-mercaptoethanol) followed by precipitation in 9% trichloroacetic acid. Precipitates were washed with acetone, dried, and resuspended in 50μL MURB protein sample buffer (100mM MES pH7.0, 1% SDS, 3M urea, 10% 2-mercaptoethanol) prior to Western analysis.

For glycosidase treatment with EndoH, cell extracts were prepared as described above, except precipitates were resuspended in 50μL Laemmli sample buffer (60mM Tris-Cl pH6.8, 2% SDS, 10% glycerol, 5% 2-mercaptoethanol), incubated 10 minutes at 95°C, and cooled to room temperature. Samples were pelleted for 60s at 13,000g and 20μL of lysate was supplemented with 1x Protease Inhibitor Mixture I (Calbiochem), followed by mock treatment or treatment with 0.75μL $EndoH_f$ (NEB) for ~16h at 37°C. Samples were incubated 5 minutes at 95°C before analysis by Western.

For cellular fractionation, cells were grown to exponential phase in SD media, and spheroplasts were prepared by incubation with 0.1M Tris, pH9.4, 50mM β-mercaptoethanol for 30 minutes followed by incubation in 1.2 M sorbitol and zymolyase 20T (4 mg/ml) for 30 minutes at 30°C. Spheroplasts were washed in 1.2 M sorbitol by centrifugation and resuspended in ice-cold lysis buffer (10 mM Triethanolamine (pH8.0), 0.8 M sorbitol, 1 mM PMSF, 1 mM EDTA and protease inhibitors) and were lysed using a glass dounce homogenizer (Whitman A). The lysate was centrifuged at 1000g for 5 min and supernatant fractions were successively centrifuged at 20,000g for 30 min, and 100,000g for 40 min. Membrane pellets were resuspended in lysis buffer. Equivalent amounts of protein from each fraction, determined by Bradford assay, were precipitated in 11% trichloroacetic acid, washed twice with cold acetone, dried, and resuspended in MURB sample buffer. For EndoH treatment of P100,000g, sample was instead resuspended in Laemmli sample buffer and treated as described above.

For antimycin A treatment, cells were grown to exponential phase in YPD or YPEG and mock-treated or treated for 4h with 20μg/mL antimycin A (Sigma) before cell extracts were prepared as described above.

Western samples were incubated for 1–2 minutes at 95°C prior to SDS-PAGE, transferred to nitrocellulose membrane, and immublotted with α-Psd1 (1:1000, antibody kind gift from S. Claypool), α-G6PDH (1:5000, Sigma-Aldrich), α-Sec61 (1:5000, gift from P. Walter laboratory), or α-Porin (1:1000, Thermo Fisher Scientific). Anti-rabbit or anti-mouse secondary antibodies conjugated to DyLight 680 or Dylight 800 (1:10000, Thermo Fisher Scientific) were used and visualized with the Odyssey Infrared Imaging System (LI-COR). Quantification of band intensities was performed with Image Studio Lite (LI-COR). Linear adjustments to images were made using Photoshop CS6 (Adobe).

Fluorescence microscopy—For fluorescence microscopy imaging, all cells were grown in SD with appropriate auxotrophic selection. Cells were grown to exponential phase, concentrated, and immobilized on microscope slides using a 3% agarose bed in growth medium. Where indicated, Δ*dpl1*Δ*psd2*Δ*psd1* cells were grown in the presence of 10mM ethanolamine. To image Δ*dpl1*Δ*psd2*Δ*psd1* cells or Δ*dpl1*Δ*psd2*Δ*psd1 +* $Psd1_{mito}$ cells without ethanolamine supplementation, exponential growth phase cells were washed and grown in SD without ethanolamine for 6h or overnight.

Images were collected using the spinning-disk module of a Marianas SDC Real Time 3D Confocal-TIRF microscope (Intelligent Imaging Innovations) fitted with a 100X, 1.46 NA objective and a Photometrics QuantEM EMCCD camera. Images were captured with SlideBook (Intelligent Imaging Innovations) and linear adjustments were made using ImageJ. Figure legends indicate when maximum intensity projections of Z-series of cells obtained using a 0.2 μm step size were shown; otherwise, single plane images were shown. Mitochondria morphological analysis was performed by manual categorization and scoring of individual cells after examining Z-series and maximum intensity projections images using ImageJ; for each independent experimental replicate, at least 70 cells per strain were quantified.

Proteomic analysis—Immunopurifications and proteomics analysis were performed as previously described (Hoppins et al., 2011), except 500 OD_{600} cells were used. Cells were grown to exponential phase in SD, resuspended in lysis buffer (20mM HEPES pH7.4, 150mM KOAc, 2mM $Mg(Ac)_2$, 1mM EGTA, 0.6M sorbitol, and 1x Protease Inhibitor Mixture I (Calbiochem), flash-frozen dropwise in liquid N_2, and lysed using a Freezer/Mill (SPEX). Cell lysates were cleared by centrifugation, cross-linked for 30 minutes with 1mM DSP (Thermo Scientific Pierce), solubilized with 1% digitonin for 30 minutes, and pelleted again. The resulting supernatant was used for purifications with 3μg α-FLAG antibody (1:1000, Sigma-Aldrich) and 50μL μMACS protein G beads (Miltenyi Biotech), and beads were isolated with μ columns and a μMACS separator (Miltenyi Biotech). Samples were eluted using on-bead trypsin digestion by applying 25μL elution buffer 1 (2M urea, 50mM Tris-Cl pH7.5, 1mM DTT, 5μg/mL trypsin) for 30 minutes followed by 2×50μL elution buffer 2 (2M urea, 50mM Tris-Cl pH7.5, 5mM chloroacetamide) and incubated overnight. Samples were quenched by addition 1μL of trifluoroacetic acid and submitted to the University of California, Davis, Genome Center Proteomics Core for LC-MS/MS analysis. Urea from the peptide samples was removed using desalting tips.

The tips were prepared by pipetting 60% acetonitrile up and down 20 times and then equilibrated with 0.1% TFA by pipetting up and down 15 times. The peptide sample was pulled through the tip 15 times before being washed with 0.1% TFA. The peptides were eluted from the tips using 100 μl of 60% acetonitrile and dried via vacuum centrifugation. Digested peptides were analyzed by LC-MS/MS on a Thermo Scientific Q Exactive Plus Orbitrap Mass spectrometer in conjunction with a Proxeon Easy-nLC II HPLC (Thermo Scientific) and a Proxeon nanospray source. The digested peptides were loaded on a 100 micron × 25 mm Magic C18 100Å 5U reverse phase trap where they were desalted online before being separated using a 75 micron × 150 mm Magic C18 200Å 3U reverse phase column. Peptides were eluted using a 140 minute gradient with a flow rate of 300nl/min. An MS survey scan was obtained for the m/z range 350–1600, MS/MS spectra were acquired using a top 15 method, where the top 15 ions in the MS spectra were subjected to HCD (High Energy Collisional Dissociation). An isolation mass window of 1.6 m/z was used for the precursor ion selection, and normalized collision energy of 27% was used for fragmentation. A fifteen second duration was used for the dynamic exclusion. Tandem mass spectra were extracted and charge state deconvoluted by Proteome Discoverer (Thermo Scientific) Charge state deconvolution and deisotoping were not performed. All MS/MS samples were analyzed using X! Tandem (The GPM, thegpm.org; version X! Tandem Alanine (2017.2.1.4)). X! Tandem was set up to search the Uniprot *Saccharomyces cerevisiae* database appended with the cRAP database of common laboratory contaminants (www.thegpm.org/crap; 114 entries) plus an equal number of reverse protein sequences assuming the digestion enzyme trypsin. X! Tandem was searched with a fragment ion mass tolerance of 20 PPM and a parent ion tolerance of 20 PPM. Carbamidomethyl of cysteine and selenocysteine was specified in X! Tandem as a fixed modification. Glu->pyro-Glu of the n-terminus, ammonia-loss of the n-terminus, gln->pyro-Glu of the n-terminus, deamidated of asparagine and glutamine, oxidation of methionine and tryptophan and dioxidation of methionine and tryptophan were specified in X! Tandem as variable modifications. Scaffold (version Scaffold_4.8.1, Proteome Software Inc., Portland, OR) was

used to validate MS/MS based peptide and protein identifications. Peptide identifications were accepted if they exceeded specific database search engine thresholds. X! Tandem identifications required at least –Log (Expect Scores) scores of greater than 1.2 with a mass accuracy of 5ppm. Protein identifications were accepted if they contained at least 2 identified peptides. Using the parameters above, the Decoy False Discovery Rate (FDR) was calculated to be 0.1% on the protein level and 0.0% on the spectrum level. Proteins that contained similar peptides and could not be differentiated based on MS/MS analysis alone were grouped to satisfy the principles of parsimony.

In vitro Psd1 activity—Psd1 assays were performed exactly as described (Raychaudhuri and Prinz, 2008). Briefly, cells were lysed by agitation with glass beads and, after spinning twice at 500 × *g* for 10 min to remove debris, 200μg of extract was incubated with 500 μM of NBD-PS (1-oleoyl-2-[12-[(7-nitro-2-1,3-benzoxadiazol-4-yl)amino]dodecanoyl]-sn-glycero-3-phosphoserine; Avanti Polar Lipids) in a total volume of 1mL. After incubation for 10 min at 37°C, lipids were extracted and analyzed by thin-layer chromatography, using the following solvent system: methanol:choloroform:acetone:water:acetic acid 10:50:20:5:15. Formation of NBD-PE was detected using a CAMAG scanner.

Lipid composition analysis—Lipids were analyzed as previously described (Kannan et al., 2017). Cells were grown in a medium containing ethanolamine to mid-logarithmic growth phase, washed and resuspended in 50 mL of media without ethanolamine. After growth for 8 h, 20 μCi of [^{3}H]acetate (American Radiolabeled Chemicals) was added and the cells were grown for 14–20 h until they reached an OD_{600} of 0.8–1.0. Cells were harvested, lysed by agitation with glass beads and lipids were extracted by adding 1.6mL of lysate to 6mL of MeOH:CHCl3 (2:1). After mixing, 2.0 mL of 0.9% NaCl was added and the organic (lower) phase was removed and dried under N_2. Lipids were separated by thin layer chromatography as described (Vaden et al., 2005). The thin layer chromatography plates (TLC Silica gel 60; Millipore Sigma) were scanned on a RITA Star Thin Layer Analyzer (Raytest) to determine the cpm per phospholipid class.

To determine the lipid composition of ER-derived membranes, strains were transformed with a plasmid encoding Sec63p fused to hemagglutinin (HA) (pRS315:Sec63-HA) (Wang et al., 2017) and grown with [^{3}H]acetate as described in the previous paragraph. Cells were washed twice with 50 mM EDTA, harvested and spheroplasts were prepared in 1.2 M sorbitol, 20 mM potassium phosphate buffer pH 7.5 and zymolyase 20T (10 mg/ml). Spheroplasts were suspended in ice-cold lysis buffer (10 mM Triethanolamine (pH8.0), 0.6 M sorbitol, 1 mM PMSF, 1 mM EDTA and protease inhibitors) and lysed with a dounce (Whitman B). The lysate was centrifuged at 500g and supernatant fractions were successively centrifuged at 10,000g for 10 min, 20,000g for 30 min and 100,000g for 40 min. The final membrane pellet was suspended in lysis buffer containing 150 mM NaCl and dounced 10 times. The homogenized membrane fractions were incubated in a 10 ml of lysis buffer contained 0.5 % BSA and anti-HA magnetic beads (Miltenyi Biotec Inc. San Diego, CA, USA) for 2h at 4°C with gentle mixing and loaded on LS Columns (Miltenyi Biotec Inc. San Diego, CA, USA) and treated with lysis buffer containing 300 mM NaCl. Lipids

were extracted from purified mitochondria as described in the previous paragraph (Lahiri et al., 2014).

QUANTIFICATION AND STATISTICAL ANALYSIS

All statistical analyses were performed in Microsoft Excel or GraphPad Prism. Statistical significance of differences in tubular mitochondrial morphology (Fig. 3D, S4B) were determined by unpaired two-tailed *t* test. Statistical significance of differences in logarithmic doubling time of yeast cultures (Fig. 3F) were determined by unpaired two-tailed *t* test. Statistical significance of difference in phospholipid composition of membranes (Fig. 3G, 4B) were determined by unpaired two-tailed *t* test. Statistical significance of differences in ER-localized Psd1 as assessed by Western analysis (Fig. 4E–4F) were determined by unpaired two-tailed *t* test.

Supplementary Material

Refer to Web version on PubMed Central for supplementary material.

Acknowledgments

We would like to thank K. Subramanian, T. Langer, and S. Claypool for providing reagents and J. Yamada for technical contributions. JN is supported by NIH grants R01 GM106019 and R37 GM097432. JF is supported by NIH grant K99 HL133372. MK and WP are supported by the Intramural Research Program of the NIDDK. JSW is supported by the Center for RNA Systems Biology, the HHMI, and by NIH grant P50 GM102706. CJ was supported by the Damon Runyon Cancer Research Foundation (DRG-2085-11).

References

Aaltonen MJ, Friedman JR, Osman C, Salin B, di Rago JP, Nunnari J, Langer T, Tatsuta T. MICOS and phospholipid transfer by Ups2-Mdm35 organize membrane lipid synthesis in mitochondria. J Cell Biol. 2016; 213:525–534. [PubMed: 27241913]

Achleitner G, Zweytick D, Trotter PJ, Voelker DR, Daum G. Synthesis and intracellular transport of aminoglycerophospholipids in permeabilized cells of the yeast, Saccharomyces cerevisiae. J Biol Chem. 1995; 270:29836–29842. [PubMed: 8530379]

Ardail D, Gasnier F, Lerme F, Simonot C, Louisot P, Gateau-Roesch O. Involvement of mitochondrial contact sites in the subcellular compartmentalization of phospholipid biosynthetic enzymes. J Biol Chem. 1993; 268:25985–25992. [PubMed: 8245031]

Baker CD, Basu Ball W, Pryce EN, Gohil VM. Specific requirements of nonbilayer phospholipids in mitochondrial respiratory chain function and formation. Mol Biol Cell. 2016; 27:2161–2171. [PubMed: 27226479]

Birner R, Burgermeister M, Schneiter R, Daum G. Roles of phosphatidylethanolamine and of its several biosynthetic pathways in Saccharomyces cerevisiae. Mol Biol Cell. 2001; 12:997–1007. [PubMed: 11294902]

Chan EY, McQuibban GA. Phosphatidylserine decarboxylase 1 (Psd1) promotes mitochondrial fusion by regulating the biophysical properties of the mitochondrial membrane and alternative topogenesis of mitochondrial genome maintenance protein 1 (Mgm1). J Biol Chem. 2012; 287:40131–40139. [PubMed: 23045528]

Elbaz-Alon Y, Rosenfeld-Gur E, Shinder V, Futerman AH, Geiger T, Schuldiner M. A dynamic interface between vacuoles and mitochondria in yeast. Dev Cell. 2014; 30:95–102. [PubMed: 25026036]

Feldheim D, Yoshimura K, Admon A, Schekman R. Structural and functional characterization of Sec66p, a new subunit of the polypeptide translocation apparatus in the yeast endoplasmic reticulum. Mol Biol Cell. 1993; 4:931–939. [PubMed: 8257795]

Flis VV, Daum G. Lipid transport between the endoplasmic reticulum and mitochondria. Cold Spring Harb Perspect Biol. 2013:5.

Friedman JR, Mourier A, Yamada J, McCaffery JM, Nunnari J. MICOS coordinates with respiratory complexes and lipids to establish mitochondrial inner membrane architecture. Elife. 2015:4.

Gardner BM, Pincus D, Gotthardt K, Gallagher CM, Walter P. Endoplasmic reticulum stress sensing in the unfolded protein response. Cold Spring Harb Perspect Biol. 2013; 5:a013169. [PubMed: 23388626]

Gohil VM, Thompson MN, Greenberg ML. Synthetic lethal interaction of the mitochondrial phosphatidylethanolamine and cardiolipin biosynthetic pathways in Saccharomyces cerevisiae. J Biol Chem. 2005; 280:35410–35416. [PubMed: 16036913]

Gulshan K, Shahi P, Moye-Rowley WS. Compartment-specific synthesis of phosphatidylethanolamine is required for normal heavy metal resistance. Mol Biol Cell. 2010; 21:443–455. [PubMed: 20016005]

Hoppins S, Collins SR, Cassidy-Stone A, Hummel E, Devay RM, Lackner LL, Westermann B, Schuldiner M, Weissman JS, Nunnari J. A mitochondrial-focused genetic interaction map reveals a scaffold-like complex required for inner membrane organization in mitochondria. J Cell Biol. 2011; 195:323–340. [PubMed: 21987634]

Horvath SE, Bottinger L, Vogtle FN, Wiedemann N, Meisinger C, Becker T, Daum G. Processing and topology of the yeast mitochondrial phosphatidylserine decarboxylase 1. J Biol Chem. 2012; 287:36744–36755. [PubMed: 22984266]

Jan CH, Williams CC, Weissman JS. Principles of ER cotranslational translocation revealed by proximity-specific ribosome profiling. Science. 2014; 346:1257521. [PubMed: 25378630]

Joshi AS, Thompson MN, Fei N, Huttemann M, Greenberg ML. Cardiolipin and mitochondrial phosphatidylethanolamine have overlapping functions in mitochondrial fusion in Saccharomyces cerevisiae. J Biol Chem. 2012; 287:17589–17597. [PubMed: 22433850]

Kainu V, Hermansson M, Hanninen S, Hokynar K, Somerharju P. Import of phosphatidylserine to and export of phosphatidylethanolamine molecular species from mitochondria. Biochim Biophys Acta. 2013; 1831:429–437. [PubMed: 23159415]

Kannan M, Lahiri S, Liu LK, Choudhary V, Prinz WA. Phosphatidylserine synthesis at membrane contact sites promotes its transport out of the ER. J Lipid Res. 2017; 58:553–562. [PubMed: 28119445]

Klug L, Daum G. Yeast lipid metabolism at a glance. FEMS Yeast Res. 2014; 14:369–388. [PubMed: 24520995]

Kojima R, Endo T, Tamura Y. A phospholipid transfer function of ER-mitochondria encounter structure revealed in vitro. Sci Rep. 2016; 6:30777. [PubMed: 27469264]

Kornmann B, Currie E, Collins SR, Schuldiner M, Nunnari J, Weissman JS, Walter P. An ER-mitochondria tethering complex revealed by a synthetic biology screen. Science. 2009; 325:477–481. [PubMed: 19556461]

Kurihara T, Silver P. Suppression of a sec63 mutation identifies a novel component of the yeast endoplasmic reticulum translocation apparatus. Mol Biol Cell. 1993; 4:919–930. [PubMed: 8257794]

Kuroda T, Tani M, Moriguchi A, Tokunaga S, Higuchi T, Kitada S, Kuge O. FMP30 is required for the maintenance of a normal cardiolipin level and mitochondrial morphology in the absence of mitochondrial phosphatidylethanolamine synthesis. Mol Microbiol. 2011; 80:248–265. [PubMed: 21306442]

Lahiri S, Chao JT, Tavassoli S, Wong AK, Choudhary V, Young BP, Loewen CJ, Prinz WA. A conserved endoplasmic reticulum membrane protein complex (EMC) facilitates phospholipid transfer from the ER to mitochondria. PLoS Biol. 2014; 12:e1001969. [PubMed: 25313861]

Nguyen TT, Lewandowska A, Choi JY, Markgraf DF, Junker M, Bilgin M, Ejsing CS, Voelker DR, Rapoport TA, Shaw JM. Gem1 and ERMES do not directly affect phosphatidylserine transport from ER to mitochondria or mitochondrial inheritance. Traffic. 2012; 13:880–890. [PubMed: 22409400]

Onguka O, Calzada E, Ogunbona OB, Claypool SM. Phosphatidylserine decarboxylase 1 autocatalysis and function does not require a mitochondrial-specific factor. J Biol Chem. 2015; 290:12744–12752. [PubMed: 25829489]

Rabl R, Soubannier V, Scholz R, Vogel F, Mendl N, Vasiljev-Neumeyer A, Korner C, Jagasia R, Keil T, Baumeister W, et al. Formation of cristae and crista junctions in mitochondria depends on antagonism between Fcj1 and Su e/g. J Cell Biol. 2009; 185:1047–1063. [PubMed: 19528297]

Raychaudhuri S, Prinz WA. Nonvesicular phospholipid transfer between peroxisomes and the endoplasmic reticulum. Proc Natl Acad Sci U S A. 2008; 105:15785–15790. [PubMed: 18836080]

Sheff MA, Thorn KS. Optimized cassettes for fluorescent protein tagging in Saccharomyces cerevisiae. Yeast. 2004; 21:661–670. [PubMed: 15197731]

Sikorski RS, Hieter P. A system of shuttle vectors and yeast host strains designed for efficient manipulation of DNA in Saccharomyces cerevisiae. Genetics. 1989; 122:19–27. [PubMed: 2659436]

Trotter PJ, Voelker DR. Identification of a non-mitochondrial phosphatidylserine decarboxylase activity (PSD2) in the yeast Saccharomyces cerevisiae. J Biol Chem. 1995; 270:6062–6070. [PubMed: 7890739]

Vaden DL, Gohil VM, Gu Z, Greenberg ML. Separation of yeast phospholipids using one-dimensional thin-layer chromatography. Anal Biochem. 2005; 338:162–164. [PubMed: 15707948]

van Meer G, Voelker DR, Feigenson GW. Membrane lipids: where they are and how they behave. Nat Rev Mol Cell Biol. 2008; 9:112–124. [PubMed: 18216768]

Vance JE. Phospholipid synthesis in a membrane fraction associated with mitochondria. J Biol Chem. 1990; 265:7248–7256. [PubMed: 2332429]

Wang X, Li S, Wang H, Shui W, Hu J. Quantitative proteomics reveal proteins enriched in tubular endoplasmic reticulum of Saccharomyces cerevisiae. Elife. 2017:6.

Westermann B, Neupert W. Mitochondria-targeted green fluorescent proteins: convenient tools for the study of organelle biogenesis in Saccharomyces cerevisiae. Yeast. 2000; 16:1421–1427. [PubMed: 11054823]

Williams CC, Jan CH, Weissman JS. Targeting and plasticity of mitochondrial proteins revealed by proximity-specific ribosome profiling. Science. 2014; 346:748–751. [PubMed: 25378625]

Highlights

- Mitochondrial phosphatidylserine decarboxylase Psd1 is also targeted to the ER
- PE generated by Psd1 at the ER and mitochondria are functionally distinct
- The organellar localization of Psd1 is modulated based on cellular metabolic needs

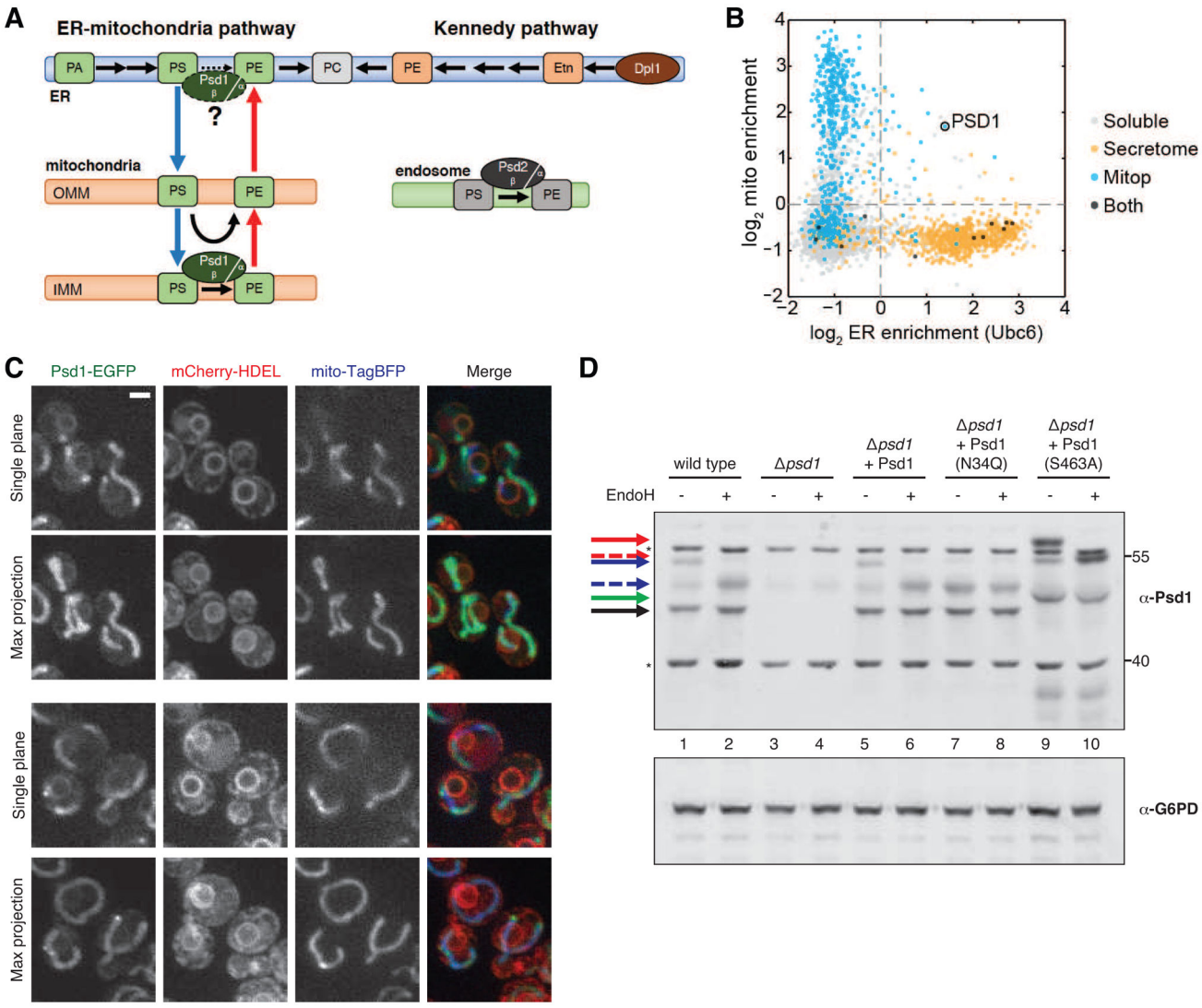

Figure 1. Psd1 is dual localized to the ER and mitochondria

(A) Schematic of yeast PE synthesis pathways. PS is decarboxylated by homologous Psd1 or Psd2. Dpl1-generated or exogenous ethanolamine (Etn) is utilized via the Kennedy pathway to produce PE at the ER. Anterograde and retrograde phospholipid transport between ER and mitochondria depicted with blue and red arrows, respectively. **(B)** A scatter plot of proteins enriched for translation in proximity to mitochondria (y-axis) and the ER (x-axis) (Williams et al., 2014). Predicted localization to the ER (orange) and mitochondria (blue). **(C)** Images of yeast cells expressing Psd1-EGFP (green), mCherry-HDEL (red), and mito-TagBFP (blue). Arrows mark Psd1 at the nuclear envelope. **(D)** Western blot analysis using the indicated antibodies of mock (-) and EndoH (+) treated lysates. Black arrow corresponds to auto-processed Psd1. Green arrow indicates non-auto-processed Psd1. Blue arrow marks glycosidase-sensitive Psd1. Red arrow indicates glycosidase-sensitive non-autocatalyzed Psd1. Dashed arrows indicate EndoH product of the corresponding colored arrow. Asterisks mark non-specific bands. Scale bars = 2 μm. See also Figure S1.

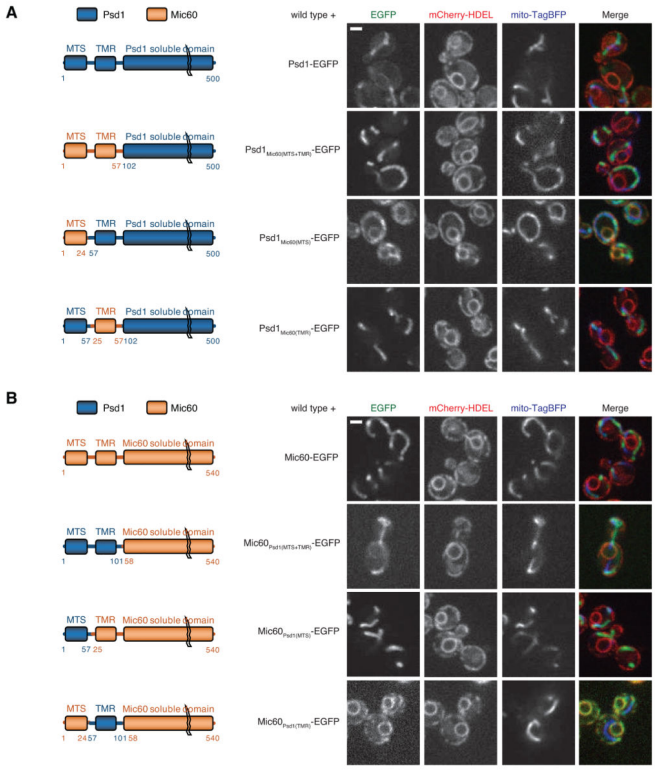

Figure 2. The Psd1 TMR is necessary and sufficient for dual ER and mitochondrial targeting

(A) Left – schematic of Psd1 (blue) chimeras with MTS and/or TMR sequences from Mic60 (orange). Right – single plane images from wild type yeast cells expressing indicated integrated EGFP-tagged Psd1 variants and mCherry-HDEL and mito-TagBFP. Arrows mark Psd1 localized to the nuclear envelope. **(B)** As in (A) for Mic60 (orange) chimeras with MTS and/or TMR sequences from Psd1 (blue). Scale bars = 2 μm.

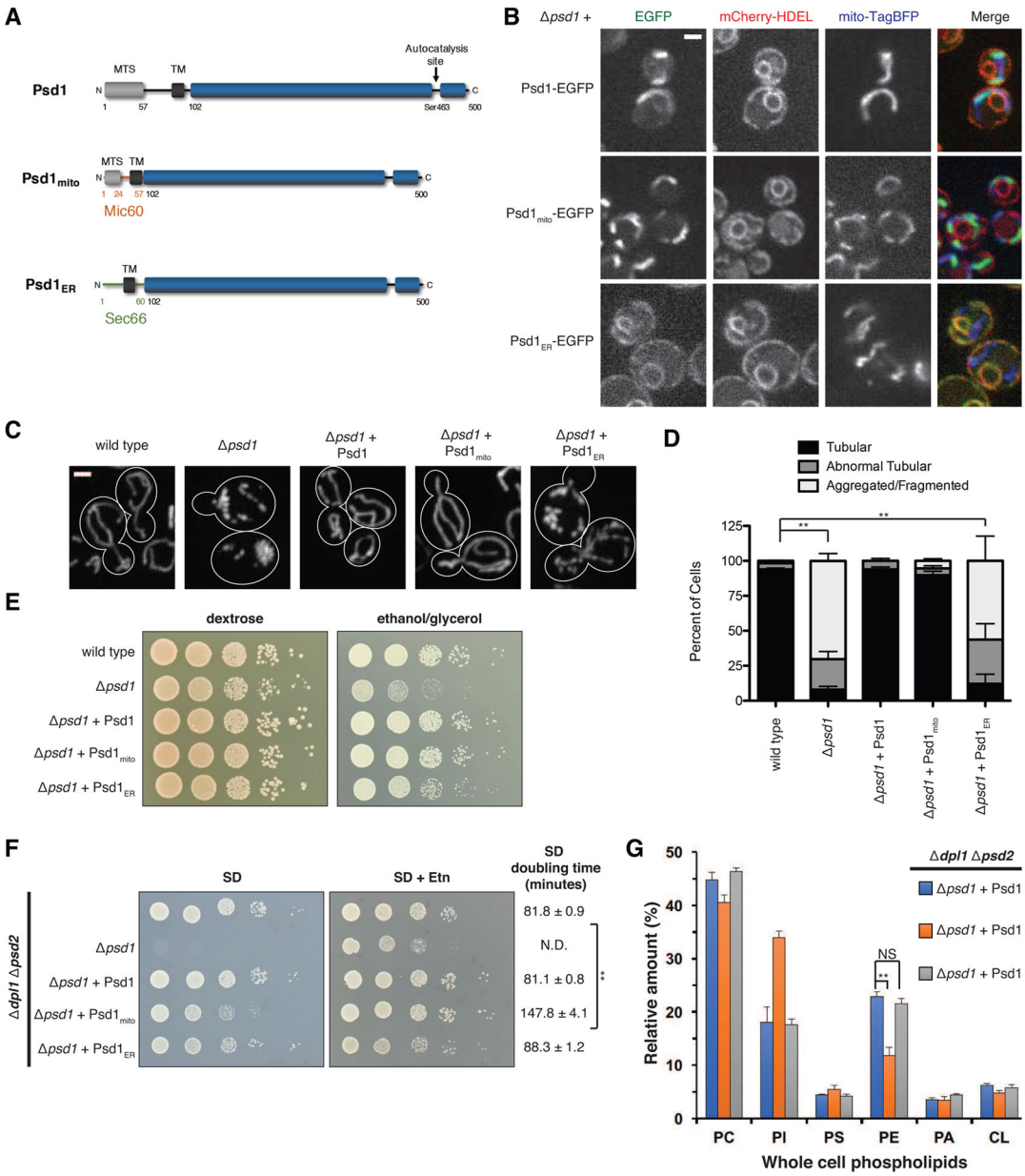

Figure 3. Mitochondrial and ER Psd1 have separable and distinct functions

(A) Schematic of mitochondria or ER chimeric Psd1 isoforms. $Psd1_{mito}$: Psd1 MTS and TMR replaced by Mic60 MTS and TMR. $Psd1_{ER:}$ Psd1 MTS and TMR replaced by Sec66 N-terminal TMR. **(B)** Localization of $Psd1_{mito}$ and $Psd1_{ER}$. Single plane images of Δ*psd1* cells expressing the indicated integrated EGFP-tagged Psd1 variant and mCherry-HDEL and mito-TagBFP. **(C)** Maximum z-projection images from indicated yeast strains expressing mito-GFP. **(D)** Mitochondrial morphology analysis of indicated strains assessed as in (C). N>70 cells per strain background from three independent experiments. Bars indicate SEM. ** p<0.001, unpaired two-tailed *t* test of tubular morphology **(E)** Serial dilutions of indicated yeast cells plated on media containing dextrose (YPD; left) and non-fermentable carbon ethanol/glycerol (YPEG; right). **(F)** Serial dilutions of the indicated yeast cells plated

on synthetic dextrose (SD) media without (left) or with (right) supplementation with 10mM Etn. Logarithmic doubling time in liquid SD media at 30°C on right as the mean ± S EM of three independent experiments. ** $p<0.001$ unpaired two-tailed *t* test **(G)** Relative percentages of indicated phospholipids as assessed by thin layer chromatography of whole cell yeast extracts from Δ*dpl1*Δ*psd2*Δ*psd1* cells expressing the indicated Psd1 variant. Bars indicate standard deviation. ** $p<0.005$ unpaired two-tailed *t* test. Scale bars = 2 μm. See also Figures S2, S3, and S4.

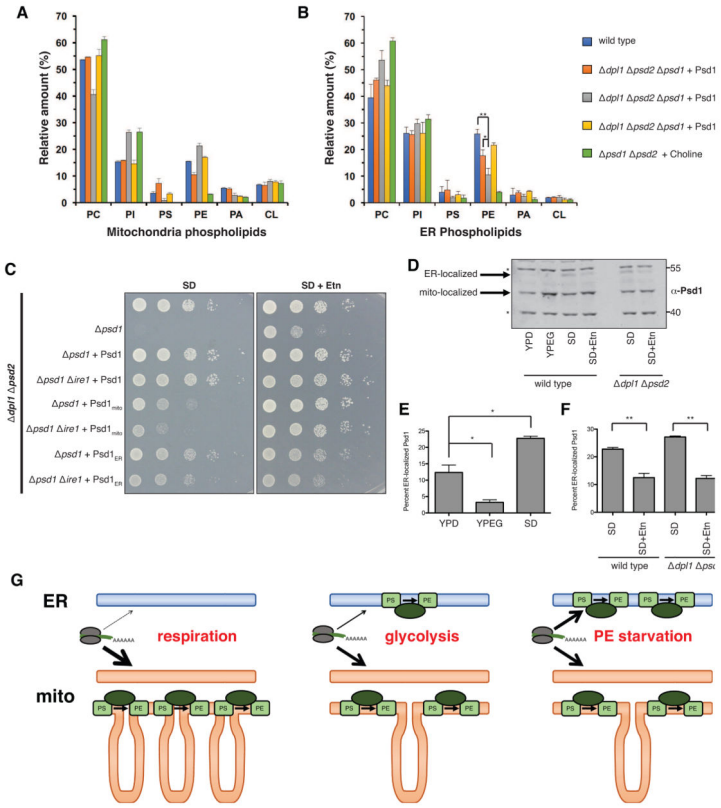

Figure 4. The steady-state organelle distribution of Psd1 changes dependent on metabolic status

(A) Relative percentages of indicated phospholipids as assessed by thin layer chromatography of purified mitochondrial extracts from the indicated strains. Bars indicate SD. **(B)** As in (A) for purified ER membranes. * $p<0.05$, ** $p<0.005$, unpaired two-tailed *t* test **(C)** Serial dilutions of indicated yeast cells on SD media without (left) or with (right) with 10mM Etn supplementation. **(D)** Western blot analysis of whole cell lysates of wild type and Δ*dpl1*Δ*psd2* cells. Bands consistent with mitochondria- and ER-localized Psd1 are indicated. Asterisks mark non-specific bands. **(E)** Graphs indicating ER-localized Psd1 from wild type cells grown in the indicated media. Bars indicate SEM of four independent experiments. * $p<0.01$, unpaired two-tailed *t* test **(F)** As in (E) for wild type and Δ*dpl1*Δ*psd2* cells grown in synthetic media with and without Etn supplementation. Bars indicate SEM of four independent experiments. ** $p<0.001$, unpaired two-tailed *t* test **(G)** Model depicting cellular modulation of ER and mitochondrial Psd1 during increased mitochondrial functional demand (decreased ER localization during respiration, left) or upon changes in phospholipid availability (increased ER localization during PE starvation, right). See also Figure S3.